InterPore JOURNAL

Original Research

HIGH-FIDELITY EXPERIMENTAL MODEL VERIFICATION FOR FLOW IN FRACTURED POROUS MEDIA

Jakub Wiktor Both[1], Bergit Brattekås[2], Eirik Keilegavlen[1], Martin A. Fernø[2,3], Jan Martin Nordbotten[1,3]

[1]Centre for Modeling of Coupled Subsurface Dynamics, Department of Mathematics, University of Bergen, Bergen, Norway; [2]Department of Physics and Technology, University of Bergen, Bergen, Norway; [3]Norwegian Research Center, NORCE, Bergen, Norway

Correspondence to:
Jakub Wiktor Both,
jakub.both@uib.no

How to Cite:
Both, J. W., Brattekås, B., Keilegavlen, E., Fernø, M., & Nordbotten, J. M. (2024). High-fidelity experimental model verification for flow in fractured porous media. *InterPore Journal*, 1(3), IPJ271124–6. https://doi.org/10.69631/

RECEIVED: 31 May 2024
ACCEPTED: 11 Sept. 2024
PUBLISHED: 27 Nov. 2024

ABSTRACT

Mixed-dimensional mathematical models for flow in fractured media have been prevalent in the modeling community for almost two decades, utilizing the explicit representation of fractures by lower-dimensional manifolds embedded in the surrounding porous media. In this work, for the first time, direct qualitative and quantitative comparisons of mixed-dimensional models are drawn against laboratory experiments. Dedicated displacement experiments of steady-state laminar flow in fractured media are investigated using both high-resolution PET images as well as state-of-the-art numerical simulations.

KEYWORDS

Flow in fractured media, Mixed-dimensional modeling, PET imaging, Wasserstein distance, Model verification

@2024 The Authors

This is an open access article published by InterPore under the terms of the Creative Commons Attribution-NonCommercial-NoDerivatives 4.0 International License (CC BY-NC-ND 4.0) (https://creativecommons.org/licenses/by-nc-nd/4.0/).

1. INTRODUCTION

The presence of fractures strongly influences both the flow and transport in porous media. As fractures are ubiquitous in many geological rocks (5) and are induced by subsurface operations (30), accurate, reliable, and verified models for fractured porous media are essential for the modeling and simulation of flow and transport in fractured porous media subsurfaces.

Since their inception approximately 20 years ago (2, 3, 25), models where fractures are represented as lower-dimensional objects (relative to the surrounding rock) have received much attention. *Such mixed-dimensional fracture models*, as we will refer to them, provide a natural framework for modeling and efficient computation related to fractured porous media. Therefore, the models have been extensively studied both in terms of their approximation properties to full *equidimensional models* (see, e.g., (25)) and their mathematical properties (see, e.g., (8)). In numerical benchmark studies, mixed-dimensional

models and their numerical discretization have been further validated against numerical discretization of equidimensional models (19).

Flow experiments have been key to understanding the process of fluid transfer between the fracture and matrix and between adjacent matrix blocks, often focusing on multi-phase flow and the balance of capillary to viscous and gravitational forces (31). Important recovery mechanisms in fractured media, such as spontaneous imbibition (26) and gravity drainage (18), have been investigated experimentally. In situ imaging has occasionally been applied to improve insight, for example, revealing the existence of wetting-phase bridges forming in vertical fractures to aid capillary continuity (4).

Despite the rich literature from both modeling and experimental perspectives, direct validation of mixed-dimensional fracture models compared to actual physical flow in fractured rock is largely missing. Consequently, key questions regarding model applicability have not been addressed, particularly those related to fracture tips and intersections. Indeed, the majority of modeling literature has emphasized the role of the fracture and its interaction with the matrix, and the modeling of fracture tips and intersections is often either treated summarily (7, 9) or simply assumed to not exist in the sense that fractures are assumed to extend to the boundary of the domain (25). In the context of discrete fracture networks, which follow a different methodology, intersections have been discussed, partially with dependence on the intersection angle (35). Considering this background, we identify three key objectives, which, to our knowledge, have not been satisfactorily addressed in previous studies:

Primarily, we ask: *Is mixed-dimensional modeling of fractured porous media a suitable framework for quantitative analysis?*

Our primary objective is substantiated through two secondary objectives. Most concretely, we address: *Does the actual physical geometry of the fracture tip impact the flow both in the fracture and surrounding matrix?* From a modeling perspective, mass balance arguments imply a no-flow condition on the fracture tip (3). Other studies have discussed non-trivial pressure and flux singularities at fracture tips depending on the fracture tip geometry (14), as well as imposing a matching flux coupling through an additional degree of freedom (34), which is postulated to be of greater relevance in the case of high transversal permeability. Notwithstanding the above references, the most common modeling choice is the flow barrier at the fracture tips. As a real physical system has no flow barrier at the fracture tips, this implies a modeling assumption that the tip geometry is completely irrelevant.

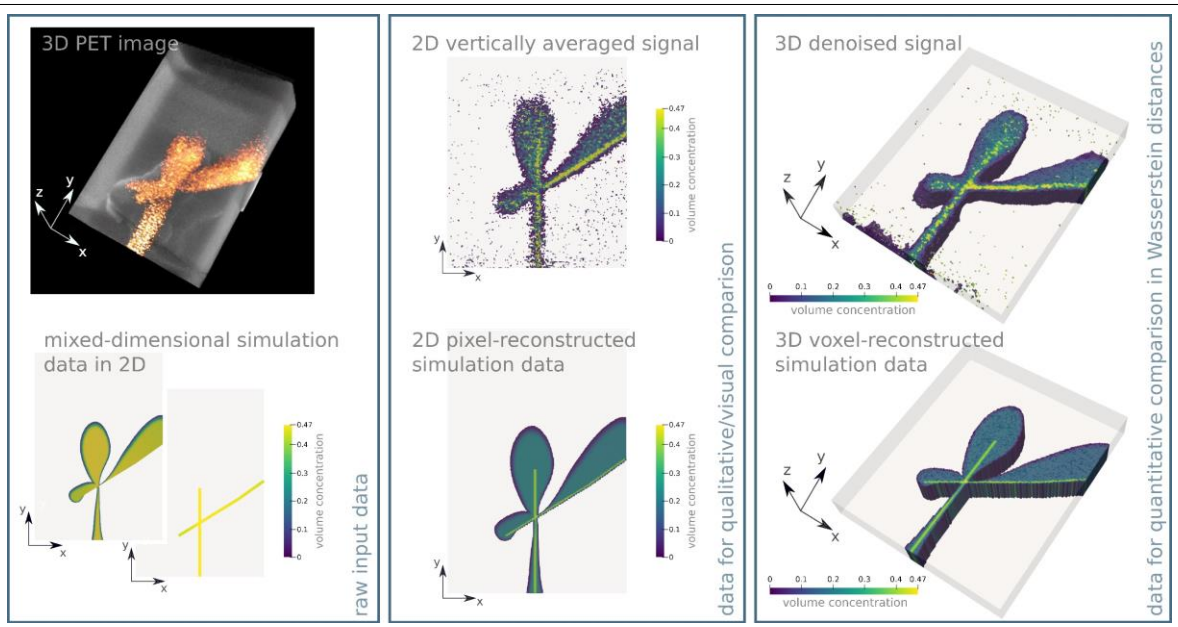


Figure 1: Schematic of available data formats considered in the verification study. PET images in vertically averaged 2D and denoised 3D views (top row); mixed-dimensional simulation data in compatible equidimensional formats (bottom row).

 DOI: https://doi.org/10.69631/ipj.v1i3nr31

Implicitly, we also address the following questions: *Is the hierarchical modeling of fracture intersections of suitable accuracy*? In the modeling literature, various constitutive modeling approaches for fracture intersections have been introduced, which are often guided by present fracture permeabilities. In addition to the imposed mass balance, the extreme cases are the pressure continuity (3, 20) and local flux/Darcy laws (20, 35). The latter consistently follows a hierarchical mixed-dimensional modeling approach, introducing pressure at the intersection, and thus pressure discontinuity. To the best of our knowledge, it has not yet been established whether these nuances matter within the context of the overall uncertainties of subsurface flows.

To address the key modeling questions identified above, we considered a series of qualitative and quantitative comparison studies between dedicated high-fidelity laboratory tracer experiments, visualized by high-resolution in situ positron emission tomography (PET) imaging (17), and numerical mixed-dimensional fracture models utilizing the state-of-the art open-source fracture flow simulator PorePy (24) (both detailed below), as illustrated in **Figure 1**.

The experiments were designed to enable the following discussion of spatiotemporal data:

- A pair of experiments were constructed, differing only in the absence and presence of added physical flow barriers in the fracture tips, which resembled the mathematical modeling assumption, thus directly addressing the impact of the fracture tip.
- Disparities of tracer plumes between experiments and mixed-dimensional fracture models were compared qualitatively through visual inspection and quantitatively in terms of Wasserstein distances, considering experiments with and without fracture intersections, thus implicitly addressing the impact of the modeling of intersections.

The remainder of this paper is organized as follows. First, we recall the principles of mixed-dimensional modeling in Section 2, which will be challenged in the present study. Dedicated laboratory tracer experiments aimed at addressing the above research questions are presented in Section 3. To enable qualitative and quantitative data comparison between the experiments and associated numerical simulations, dedicated data processing and analysis are required, as introduced in Section 4. Finally, a detailed model verification study is presented in Section 5, and the conclusions are drawn in Section 6.

2. MIXED-DIMENSIONAL CONCEPTUALIZATION OF FRACTURES

The dimensional reduction and representation of fractures as lower-dimensional objects has three central implications: the introduction of (I) mixed-dimensional geometry, (II) mixed-dimensional representation of physical fields, and (III) meaningful model equations coupling the physics between adjacent objects of varying dimensions (8, 9, 25). This is exemplified in the context of the flow and tracer transport.

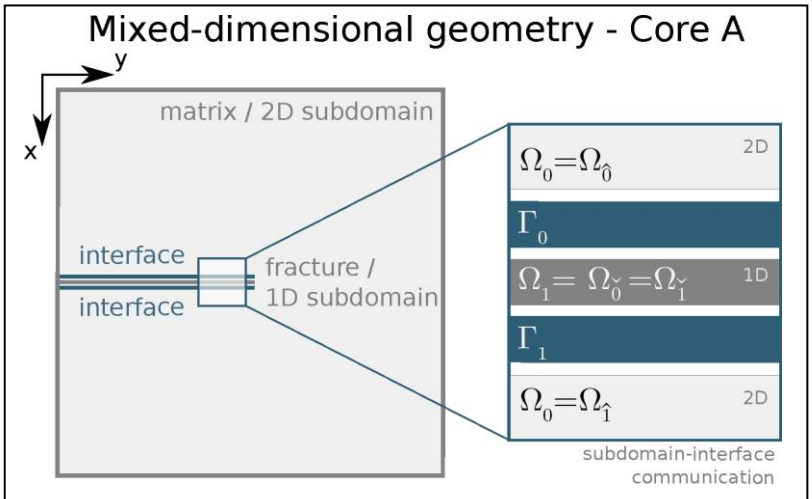


Figure 2: Conceptual mixed-dimensional representation of Core A, cf. **Figure 3** in 2D with subdomains $\{\Omega_i\}_{i\epsilon I}$ (gray) and interfaces $\{\Gamma_j\}_{j\epsilon J}$ (blue).

2.1. Mixed-dimensional geometry (I)

Fractures are three-dimensional geometrical features with high aspect ratios. Compared to the dimensions of the surrounding

 DOI: https://doi.org/10.69631/ipj.v1i3nr31

matrix, the width of the cross-section is several orders of magnitude smaller. Hence, from a geometrical standpoint, a lower-dimensional representation of the fractures appears natural. The argumentation recursively continuous to fracture intersections. Consequently, a general fractured medium $\Omega \subset \mathbb{R}^N$ can be conveniently described as a hierarchy of mixed-dimensional geometries, $\{\Omega_i\}_{i\epsilon I}, \mathrm{I} := \{1, \dots, m\}$, with the matrix as a subdomain of the ambient dimension, fractures of codimension 1 (planes), intersections of fractures of codimension 2 (lines), and intersections of codimension 3 (points) (9). Interfaces, $\{\Gamma_j\}_{j\in J}, J := \{1, \dots, M\}$, between subdomains of co-dimension 1 allow for data exchange via suitable projections. Examples are shown in **Figure 2**.

2.2. Mixed-dimensional fields (II)

As a result of the dimensional reduction (25), physical fields originally defined in the equidimensional geometry receive distinct representations on each subdomain, collected in the form of a mixed-dimensional field. In the context of flow and transport, the mixed-dimensional fluid pressure $\{p_i\}_{i\in I}$ and tracer concentration $\{c_i\}_{i\in I}$ are defined.

2.3. Mixed-dimensional equations (III)

A complete mathematical description of the flow on mixed-dimensional geometries requires the assignment of equations on both the subdomains and connecting interfaces. Starting from an equidimensional model, these can be derived by averaging or integrating over the fracture apertures. In addition, postulation of closure relations is required. A key feature of the prototypical model is the conceptually identical treatment of each dimension.

The focus of this study lies on the incompressible, quasi-static, laminar flow in porous media. Based on the fundamental principle of mass conservation, together with Darcy's law, the governing equation for flow on the subdomain $\Omega_i, i \in I$, is given by (**Eq. 1**):

$$\nabla_\parallel \cdot \left(-v_i \mu^{-1} K_{\parallel,i} \nabla_\parallel p_i\right) = f_i + \sum\nolimits_{j\in S_i} \lambda_j \tag{1}$$

where v_i is the specific volume resulting from dimension reduction (equal to 1 at the ambient dimension, the fracture width for fractures, their product for intersections etc.), $\nabla_\parallel$ is the tangential differential operator (void on 0-dimensional subdomains), $K_{\parallel,i}$ is the tangential permeability tensor, μ is the dynamic viscosity, f_i is the volumetric source, S_i identifies neighboring interfaces towards subdomains of one dimension higher (empty for subdomains of ambient dimension) and $\{\lambda_j\}_{j\in S_i}$ are associated interface fluxes. The tangential permeability $K_{\parallel,i}$ simply equals the matrix permeability at ambient dimension; for fractures and intersections, we choose a cubic law associated with perfect Poiseuille flow (7), that is, we set $K_{\parallel,i} = \frac{v_i^2}{12}$ for fractures.

On neighboring pairs of lower- and higher-dimensional subdomains, $\Omega_j = \Omega_i$ and Ω_j (with $\widetilde{\cdot}$ and $\widehat{\cdot}$ associating subdomains with interface $\cdot$, cf. **Fig. 2**), the flux across their interface Γ_j respectively appears as source terms as in **Equation 1** and Neumann boundary condition (**Eq. 2**):

$$\left(-\mu^{-1} K_{\parallel,j} \nabla_\parallel p_j\right) \cdot n_j = \lambda_j \text{ on } \partial\Omega_j \cap \Gamma_j \tag{2}$$

where n_j denotes the outer normal vector onto $\partial\Omega_j \cap \Gamma_j$. Based on a linearity assumption, the flux λ_j across Γ_j follows a Darcy-like law, introducing the normal permeability κ_j, which is inversely correlated to the intrinsic aperture a_j (9)), effectively representing a discrete normal derivative (25), (**Eq. 3**):

$$\lambda_j = -\mu^{-1} \kappa_j (p_j - p_j), \qquad \kappa_j = v_j K_{\parallel,j} / (\tfrac{1}{2} a_j) \tag{3}$$

Boundary conditions are assigned to close the system. At the external boundaries of the host medium Ω, the pressure and flux boundary conditions depend on the use case. At the internal boundaries, i.e., fracture tips, we employ the widely used consensus and impose no-flow conditions (**Eq. 4**):

$$\left(-\mu^{-1} K_{\parallel,i} \nabla_\parallel p_i\right) \cdot n_i = 0 \tag{4}$$

 DOI: https://doi.org/10.69631/ipj.v1i3nr31

With these modeling choices, all parameters are defined exclusively in terms of the matrix permeability and fracture apertures; thus, our model, as applied in this study, contains no free tuning parameters.

Following the same methodology, passive tracer transport in fractured media can be similarly modelled as mixed-dimensional advection-dispersion (21). The tracer transport in subdomain $\Omega_i, i \in I$, is governed by (**Eq. 5**):

$$v_i\left[\phi_i \partial_t c_i + \nabla_\parallel \cdot \left(c_i q_i - D_{\parallel,i} \nabla_\parallel c_i\right)\right] = h_i + \sum_{j \in S_i} \eta_j \tag{5}$$

where ϕ_i is the porosity, $q_i = -\mu^{-1} K_{\parallel,i} \nabla_\parallel p_i$ is the advective flux, $D_{\parallel,i}$ is the tangential dispersion (tensor), and h_i is the volumetric source term. In this work, the dispersion $D_{\parallel,i}$ follows an anisotropic model, decomposing in longitudinal dispersion $D_{\mathrm{L},\parallel,i} = \alpha_{\mathrm{L}} |q_i|$ and transversal dispersion $D_{\mathrm{T},\parallel,i} = \alpha_{\mathrm{T}} |q_i|$, see e.g. (15). The system is closed following the same modelling principles as for mixed-dimensional flow, introducing advective-diffusive interface fluxes η_j.

Remark 1 (Numerical approximation). Numerical simulations allow for the approximation of mixed-dimensional models, such as **Equation 1** to **Equation 5**, for highly complex geometries. For this study, the choice of numerical discretization is not essential, as long as it is locally conservative, consistent, and stable across all dimensions. This ensures that, by choosing a sufficiently fine grid, the approximation error is negligible compared to the modeling error. In this study, a locally conservative finite volume discretization is employed with diffusive fluxes approximated with the MPFA method (1, 29), yet tailored to mixed-dimensional models following the unified framework in (28). Convective fluxes are approximated using first-order upstream weighting (16). For the implementation, the open-source software framework PorePy (24) is used, which provides mass-conservative finite volume discretizations that have been extensively validated against the model equations through participation in code comparison studies (6) and by a posteriori error analysis (37). We highlight a series of other numerical modeling approaches, for which we expect similar results, given that the meshes are sufficiently fine. This includes conforming approaches (13, 22, 23), and nonconforming approaches (20, 33, 36), see also the benchmarking studies (6, 19), and references therein.

3. LABORATORY TRACER EXPERIMENTS OF FRACTURE FLOW

For the subsequent model verification study aimed at addressing the above research questions, dedicated laboratory tracer experiments were conducted. For all four setups, as illustrated in **Figure 3**, a cuboid Bentheimer sandstone core material was used and cut using a diamond saw blade to create thin smooth fractures. Aiming at investigating the fracture tips and intersections, four configurations were chosen: two geometries with a simple cut (Core A and Core B); Core A but with the fracture tip closed by a metal splinter (Core A*) resembling an actual physical flow barrier, thus imitating the mathematical model equation (**Eq. 4**); and a geometry with a simple fracture network consisting of two intersecting fractures (Core C), realized by assembling the rock pieces with epoxy on a fixed plate.

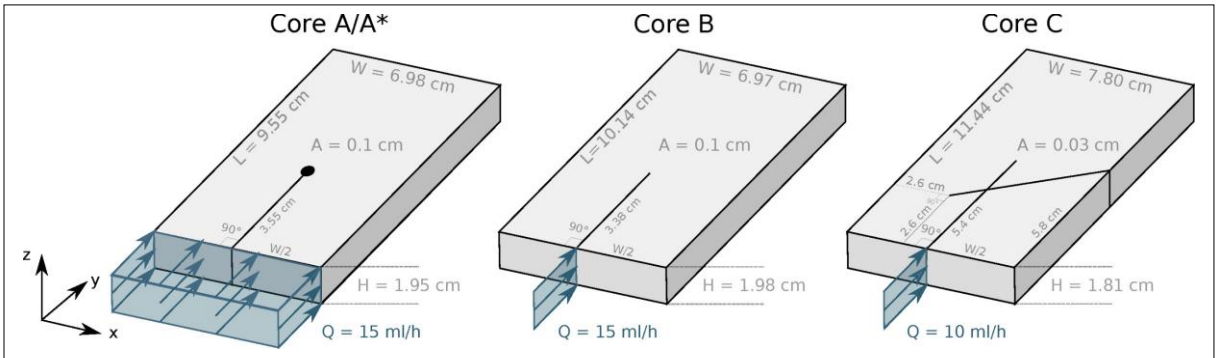


Figure 3: Geometrical specifications of Cores A/A* (A* but with splinter in tip), B, and C, including length (L), width (W), height (H), fracture aperture (A); injection strategy and rate (Q) (blue).

 DOI: https://doi.org/10.69631/ipj.v1i3nr31

Each core sample was treated as homogeneous and isotropic. Based on independent displacement experiments using intact core material, effective hydraulic matrix properties (porosity, permeability, and dispersion) were determined, see **Table 1** for respective values.

Table 1: Material properties at ambient dimension.

Property (Unit)	Core A/A*	Core B	Core C
ϕ	0.232	0.221	0.211
$K_{\parallel}[\mathrm{D}]$	1.9±0.1	1.8±0.07	1.5±0.1
$\alpha_{\mathrm{L}}[\mathrm{m}]$	7e-4	7e-4	7e-4
$\alpha_{\mathrm{T}}[\mathrm{m}]$	0.2 α_{L}	0.2 α_{L}	0.2 α_{L}

The rock cores were initially saturated with 3.5% NaCl brine (viscosity μ =1.09cP at ambient temperature) under vacuum. Brine was thereafter injected into the inlet of each core, using slightly different conditions; **Figure 3** shows the injection across the entire inlet or directly into the fracture, while the outlet end face is open to flow and fluid is produced at atmospheric pressure. Polyoxymethylene end-pieces were machined and attached to the inlet and outlet end-faces to define and facilitate injection and extraction. The remaining core faces were impervious to fluid flow owing to the use of epoxy.

High-resolution in situ PET imaging was used to track the flow patterns, cf. **Figure 1**. The cores were placed in a high-resolution, multimodal PET-CT scanner and radioactive ^{18}F-FDG-labelled brine was used as the injection fluid. Low concentrations, which are still detectable by PET, are used to avoid notably altering the fluid density and viscosity. Consequently, the experiments were quasi-2D.

4. DATA PROCESSING AND ANALYSIS

The model verification in Section 5 relies on visual and quantitative data comparisons of both experimental and corresponding numerical data. The tools for data processing and analysis employed the open-source Darcy-Scale Image Analysis toolbox DarSIA (27), as detailed below.

4.1. Unified Data Format for Qualitative Comparison

The foundation of the model validation study is a direct comparison of laboratory PET data and the corresponding mixed-dimensional simulation data. Such a comparison solicits a common ground, chosen here as a time-series of volumetric (Darcy-scale) concentration with respect to the matrix, cf. **Figure 1**. We note the omission of pressure data, as a PET-CT scanner is not equipped to measure the pressure within the 3D space. Therefore, the tracked and simulated tracer concentrations were the only dense quantities available for a direct comparison. While the simulation data undergoes mass-conservative equidimensional reconstruction, the sparse PET signal of the experimental data requires space-time smoothing to extract the Darcy-scale concentration data. To this end, snapshots were obtained from the dynamic 4D PET images through signal accumulation over 4D space-time cubes (60 seconds × 0.4 mm voxels); total variation denoising was used for simultaneous shape-preserving denoising and inpainting, and signal rescaling allowed for matching the known injection rate, finally defining the cleaned data sets used in this study. This workflow retains the quality of the dataset and regularizes the signal in the order of the measurement error (27), (please also refer to Section B.2 in the Supplementary Material, available online here). Dimension reduction (3D to 2D) was applied to enable visual comparison of the (almost) plane symmetric tracer plumes.

4.2. Dissimilarity metric for quantitative comparison

In addition to assessing the qualitative match via visual comparison of tracer plumes, the disparity between the concentration data can be quantified in terms of the 1-*Wasserstein distance* (11) (Earth Mover's Distance (32)). It explicitly measures the mass distance required to transport a tracer density from one location to another in the form of a mass-conservative flux field (here termed *Wasserstein flux*). For universal interpretation, we employ a relative distance with the reference value given by the average mass distance of the current concentration profile from the injection boundary (see Section B.1 in the Supplementary Material for the details, available online here). The relative 1-Wasserstein distance allows for the discussion of experimental variability.

 DOI: https://doi.org/10.69631/ipj.v1i3nr31

Remark 2 (Experimental variability). To obtain a baseline estimate of the deviation of the experiment from its design, we consider the deviation in the tracer distributions for Cores A, A*, and B, from a symmetric distribution (the experimental design has a North-South symmetry axis), in terms of a (relative) Wasserstein distance. The identical operating conditions across all experiments justify its interpretation as a proxy for measurement uncertainty and the reduction to a characteristic value (of the order of 0.046 ± 0.013, cf., Sec. B.3 in the Supplementary Material available online). We emphasize that this should be seen as a lower bound on the actual experimental uncertainty, as it does not account for any experimental artifacts that are not symmetry-breaking (impact of epoxy casing, imperfections in cutting of fracture, variability in the flow pumps, etc.).

5. QUALITATIVE AND QUANTITATIVE COMPARISON OF EXPERIMENTS AND SIMULATIONS

Access to experimental data (12) and the corresponding accurate numerical simulation data (10), as described above, allows for model verification through direct data comparison. The fracture tips and intersections are discussed separately.

5.1. Direct assessment of the impact of fracture tip geometry

To probe the validity of the central modeling assumption of a no-flow condition in the fracture tip (**Eq. 4**), the focus lies on comparing the laboratory experiments conducted using the Cores A and A*, recalling that these are identical from a modeling perspective. The Wasserstein distance for different time steps between the experimental data of the two different experimental series as well as the simulation data is employed to assess the fit. The relative distances are displayed in **Figure 4**, together with the Wasserstein

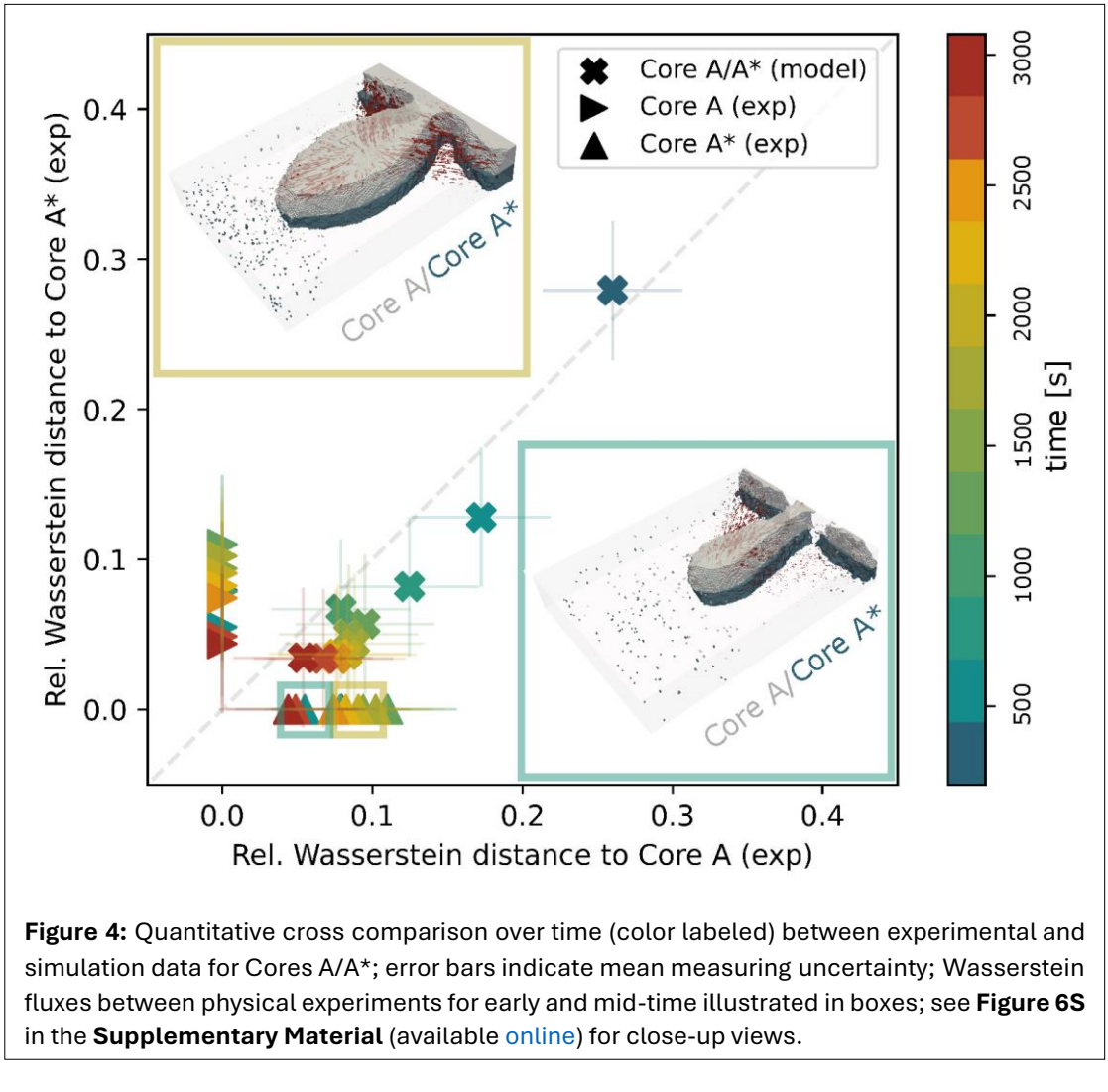


Figure 4: Quantitative cross comparison over time (color labeled) between experimental and simulation data for Cores A/A*; error bars indicate mean measuring uncertainty; Wasserstein fluxes between physical experiments for early and mid-time illustrated in boxes; see **Figure 6S** in the **Supplementary Material** (available online) for close-up views.

 DOI: https://doi.org/10.69631/ipj.v1i3nr31

flux for a single time step, illustrating the structure of the error. Considering only the experimental results (triangles), we observe that after an early time transient, the deviation between the two experiments is of the order of 3-10%, which is comparable to the experimental uncertainty. In contrast to the experiments with the simulation results (indicated by crosses), we see that (within experimental uncertainty) the mathematical model is equally close to either of the two experiments, and at later times is as close to the experiments as the variability between them. Thus, we make two observations.

1. The equidistance between the simulation and the two experiments indicates that the dominant modeling error cannot be ascribed to the treatment of the fracture tip.
2. Clustering of the experiments and the simulation within a 5-10% relative error implies that the modeling error is within the general uncertainty associated with the reproducibility of the experiment.

A qualitative visual comparison, as illustrated in **Figure 5**, supports the assessment of close agreement between the modeling and experimental results. The discrepancies can be summarized as follows. For all cores, slight dispersive overshoots and undershoots can be observed at single locations along the front (highlighted), which are not reproduced by the simulations. However, for all cases with a single fracture (Core A/A* and Core B, being equivalent to Core A apart from the boundary condition), the general structure of the concentration distribution is comparable between simulation and experiment, with the largest discrepancies for Core A/A* near the inlet boundaries, indicating that the realization of the boundary conditions may be of greater significance than the modeling of the fracture tip. We stress that a certain degree of uncertainty will be present in the experimentally imposed inlet boundary conditions because the manufactured inlet end-face converts a point to an approximated uniform face

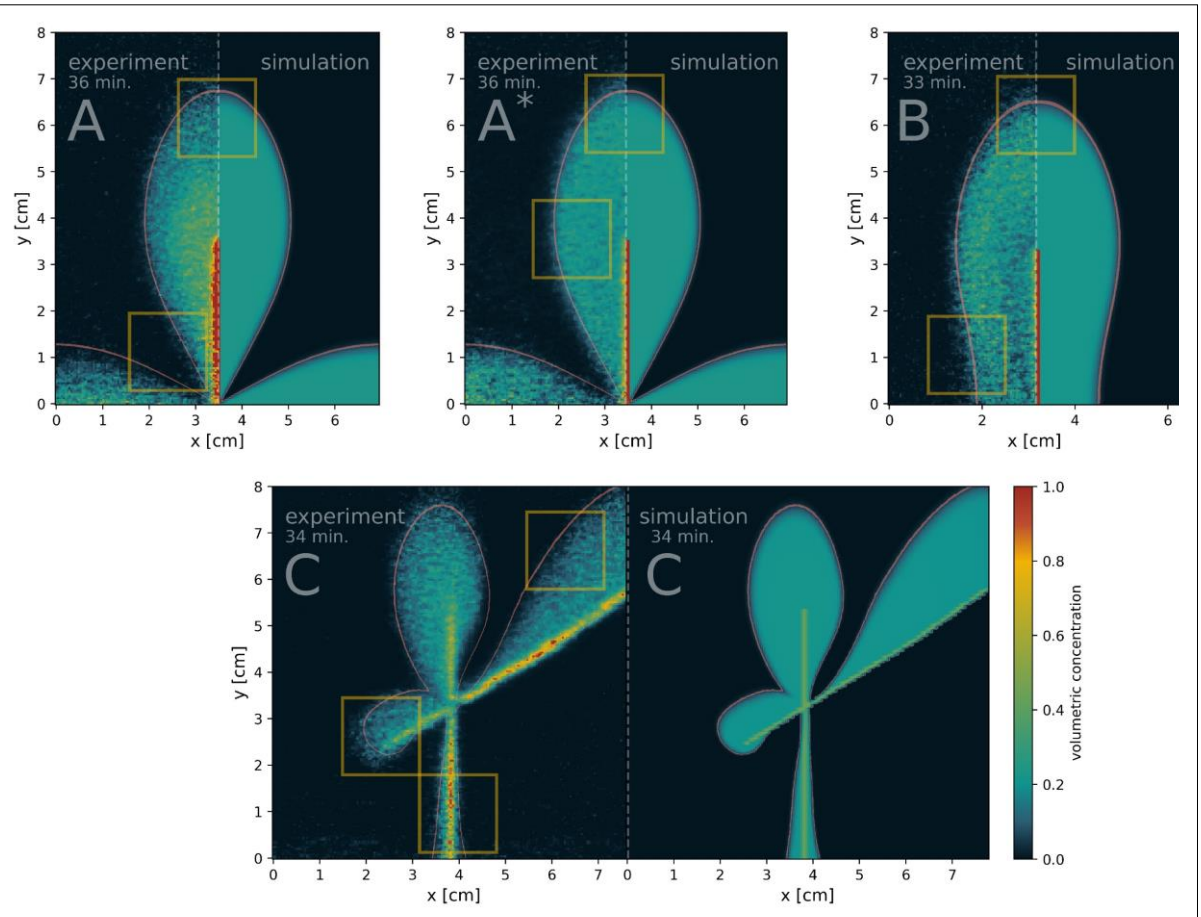


Figure 5: Side-by-side comparison of concentration plumes from experimental and simulation data for Cores A, A*, B, and C. Yellow boxes highlight regions with subtle discrepancies discussed further in the text, and a red 5% contour line on the simulated tracer data aids in visual comparison.

 DOI: https://doi.org/10.69631/ipj.v1i3nr31

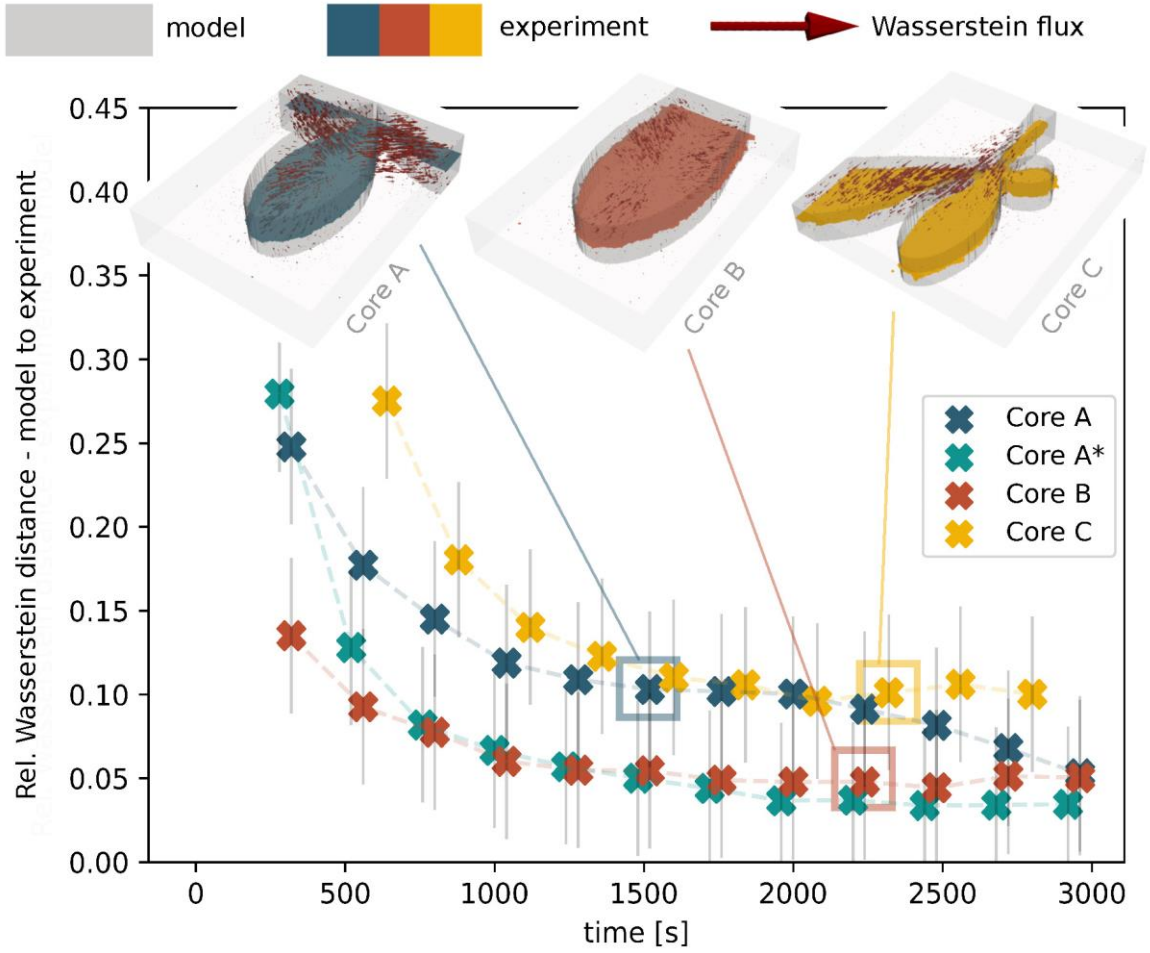


Figure 6: Temporal evolution of Wasserstein distances comparing the model with corresponding experiments, with error bars representing the mean measurement uncertainty. Wasserstein fluxes are shown for individual time steps.

source (cf. Sec. 3). This aligns with the quantitative analysis of Cores A/A∗ and B (**Fig. 6**), where Core B, with the simplest boundary condition, has the closest fidelity between experiment and simulation. Further snapshots are displayed in Section A of the **Supplementary Material** (available online).

5.2. Implicit assessment of impact of fracture intersections

Fracture intersections have numerous structural parameters that prohibit a full direct comparison in the experimental setting. Therefore, we must rely on more implicit arguments by constructing a single core with non-orthogonal crossing. We first return to the qualitative impressions gained from **Figure 5**. The impression is that all the main features of the tracer distribution associated with Core C are reproduced by the simulation, including the asymmetric flow out of the fractures and the nontrivial distribution of the tracer near the intersection and the fracture tips. The time chosen in **Figure 5** is representative; snapshots for other times are provided in Section A of the **Supplementary Material** (available online). To support this qualitative comparison, Wasserstein distances are again computed between the regularized laboratory data and the corresponding simulation data, cf. **Figure 6**. The relative distances again substantiate the qualitative comparison above, with the discrepancy between the simulation and model for Core C being within a factor of 2 of the other cores, despite the increase in geometric complexity. Inspection of the associated Wasserstein fluxes (insets) allows for the interpretation of the deviations, emphasizing the unbalanced fluid distribution among the fractures in Core C. Based on the available data, it is not possible to determine whether these deviations are due to experimental imperfections or modeling.

 DOI: https://doi.org/10.69631/ipj.v1i3nr31

6. CONCLUSION

In conclusion, we return to our primary objective, that is, by means of careful experiments, assess the validity of mixed-dimensional modeling of fractured porous media. Overall, across all four experimental setups, we see a relative error of the order of 10% between the simulation and model, which in the context of the complexity associated with transport in fractured porous media (5), we consider it to be very satisfactory. As such, our overall assessment is that the data and simulations presented herein provide a strong experimental justification for the applicability of mixed-dimensional modeling concepts in fractured porous media. Finally, we highlight the availability of the laboratory data (12) which could also serve as basis for future validation of equidimensional fracture-matrix models, exceeding the Darcy-Darcy reduced order models as discussed here.

Conceptually, mixed-dimensional models naturally extend to geometries featuring non-planar fractures with varying apertures and rough surfaces. While the present study has focused on an idealized setup aiming to thoroughly evaluate the mathematical model under reduced uncertainty, future validation in a more complex setting would be of high interest. This includes more complex fracture networks with dominating interaction between fractures, inspired by geological field applications.

STATEMENTS AND DECLARATIONS

Supplementary Material

The following supplementary material is available for download here with this paper: Additional snapshots substantiating the model verification and further information on the Wasserstein metric entering the quantitative analysis and error quantities.

Author Contributions

Jakub W. Both: Methodology, Data curation, Investigation, Software, Visualization, Writing- Original draft preparation. Bergit Brattekås: Data curation, Investigation, Visualization, Writing- Reviewing and Editing. Eirik Keilegavlen: Writing- Reviewing and Editing. Martin A. Fernø: Conceptualization, Writing- Reviewing and Editing. Jan M. Nordbotten: Conceptualization, Writing- Reviewing and Editing, Funding acquisition.

Conflicts of Interest

There are no conflicts of interest to declare.

Data, Code & Protocol Availability

The DICOM data of the PET images is available at (12). The runscripts for PorePy simulation and DarSIA analysis are found under (10).

Funding Received

This work is funded by the UoB Akademia-project FracFlow.

ORCID IDs

Jakub Wiktor Both https://orcid.org/0000-0001-6131-4976
Bergit Brattekås https://orcid.org/0000-0002-4287-2611
Eirik Keilegavlen https://orcid.org/0000-0002-0333-9507
Martin A. Fernø https://orcid.org/0000-0002-5745-0825
Jan Martin Nordbotten https://orcid.org/0000-0003-1455-5704

REFERENCES

1. Aavatsmark, I. (2002). An introduction to multipoint flux approximations for quadrilateral grids. *Computational Geosciences*, 6(3), 405–432. https://doi.org/10.1023/A:1021291114475
2. C., Jaffré, J., Roberts, J. E., and Serres, C (2002). Modeling fractures as interfaces for flow and transport. In: Chen, Z., Ewing, R. E. (Eds.). *Fluid Flow and Transport in Porous Media: Mathematical and Numerical Treatment*. American Mathematical Society, Vol. 295. https://doi.org/10.1090/conm/295
3. Angot, P., Boyer, F., & Hubert, F. (2009). Asymptotic and numerical modelling of flows in fractured porous media. *ESAIM: Mathematical Modelling and Numerical Analysis*, 43(2), 239–275. https://doi.org/10.1051/m2an/2008052
4. Aspenes, E., Ersland, G., Graue, A., Stevens, J., & Baldwin, B. A. (2008). Wetting phase bridges establish capillary continuity across open fractures and increase oil recovery in mixed-wet fractured chalk. *Transport in Porous Media*, 74(1), 35–47. https://doi.org/10.1007/s11242-007-9179-3
5. Berkowitz, B. (2002). Characterizing flow and transport in fractured geological media: A review. *Advances in Water Resources*, 25(8–12), 861–884. https://doi.org/10.1016/S0309-1708(02)00042-8
6. Berre, I., Boon, W. M., Flemisch, B., Fumagalli, A., Gläser, D., et al. (2021). Verification benchmarks for single-phase flow in three-dimensional fractured porous media. *Advances in Water Resources*, 147, 103759. https://doi.org/10.1016/j.advwatres.2020.103759
7. Berre, I., Doster, F., & Keilegavlen, E. (2019). Flow in fractured porous media: A review of conceptual models and discretization approaches. *Transport in Porous Media*, 130(1), 215–236. https://doi.org/10.1007/s11242-018-1171-6
8. Boon, W. M., Nordbotten, J. M., & Vatne, J. E. (2021). Functional analysis and exterior calculus on mixed-dimensional geometries. *Annali Di Matematica Pura Ed Applicata* (1923 -), 200(2), 757–789. https://doi.org/10.1007/s10231-020-01013-1
9. Boon, W. M., Nordbotten, J. M., & Yotov, I. (2018). Robust discretization of flow in fractured porous media. *SIAM Journal on Numerical Analysis*, 56(4), 2203–2233. https://doi.org/10.1137/17M1139102
10. Both, J., Brattekås, B., Keilegavlen, E., Martin, F., & Nordbotten, J. M. (2023). Simulation and data analysis: High-fidelity experimental model verification for flow in fractured porous media [Computer software]. Zenodo. https://doi.org/10.5281/zenodo.10410227
11. Both, J. W., Facca, E., and Nordbotten, J. M. (2023). Iterative finite volume approximation of the 1-Wasserstein distance. [Manuscript in preparation].
12. Brattekås, B., Both, J., Keilegavlen, E., Fernø, M., & Nordbotten, J. M. (2023). Dataset: High-fidelity experimental model verification for flow in fractured porous media [Dataset]. Zenodo. https://doi.org/10.5281/zenodo.10409926
13. Brenner, K., Hennicker, J., Masson, R., & Samier, P. (2016). Gradient discretization of hybrid-dimensional Darcy flow in fractured porous media with discontinuous pressures at matrix–fracture interfaces. *IMA Journal of Numerical Analysis*, drw044. https://doi.org/10.1093/imanum/drw044
14. Chen, K. P., Jin, Y., & Chen, M. (2013). Pressure-gradient singularity and production enhancement for hydraulically fractured wells. *Geophysical Journal International*, 195(2), 923–931. https://doi.org/10.1093/gji/ggt272
15. De Marsily, G. (1986). Quantitative hydrogeology. United States. Paris School of Mines, Fontainebleau.
16. Eymard, R., Thierry, G., and Herbin, R. (2000). *Finite Volume Methods. Handbook of Numerical Analysis*, 7:713–1018, 2000.
17. Fernø, M. A., Gauteplass, J., Hauge, L. P., Abell, G. E., Adamsen, T. C. H., & Graue, A. (2015). Combined positron emission tomography and computed tomography to visualize and quantify fluid flow in sedimentary rocks. *Water Resources Research*, 51(9), 7811–7819. https://doi.org/10.1002/2015WR017130
18. Firoozabadi, A. (2000). Recovery mechanisms in fractured reservoirs and field performance. *Journal of Canadian Petroleum Technology*, 39(11). https://doi.org/10.2118/00-11-DAS
19. Flemisch, B., Berre, I., Boon, W., Fumagalli, A., Schwenck, N., Scotti, A., Stefansson, I., & Tatomir, A. (2018). Benchmarks for single-phase flow in fractured porous media. *Advances in Water Resources*, 111, 239–258. https://doi.org/10.1016/j.advwatres.2017.10.036B.
20. Flemisch, B., Fumagalli, A., and Scotti, A. (2016). A review of the XFEM-based approximation of flow in fractured porous media. In: Ventura, G., Benvenuti, E. (Eds). *Advances in Discretization Methods*. Springer Nature, 47–76.
21. Fumagalli, A. and Scotti, A. (2012). A reduced model for flow and transport in fractured porous media with non-matching grids. In: Cangiani, A., Davidchack, R., Georgoulis, E., Gorban, A., Levesley, J., Tretyakov, M. (eds). *Numerical Mathematics and Advanced Applications*. Springer, 499–507.
22. Hoteit, H., & Firoozabadi, A. (2005). Multicomponent fluid flow by discontinuous Galerkin and mixed methods in unfractured and fractured media. *Water Resources Research*, 41(11), 2005WR004339. https://doi.org/10.1029/2005WR004339

23. Hoteit, H., & Firoozabadi, A. (2008). An efficient numerical model for incompressible two-phase flow in fractured media. *Advances in Water Resources*, 31(6), 891–905. https://doi.org/10.1016/j.advwatres.2008.02.004
24. Keilegavlen, E., Berge, R., Fumagalli, A., Starnoni, M., Stefansson, I., Varela, J., & Berre, I. (2021). PorePy: An open-source software for simulation of multiphysics processes in fractured porous media. *Computational Geosciences*, 25(1), 243–265. https://doi.org/10.1007/s10596-020-10002-5
25. Martin, V., Jaffré, J., & Roberts, J. E. (2005). Modeling fractures and barriers as interfaces for flow in porous media. *SIAM Journal on Scientific Computing*, 26(5), 1667–1691. https://doi.org/10.1137/S1064827503429363
26. Mason, G., & Morrow, N. R. (2013). Developments in spontaneous imbibition and possibilities for future work. *Journal of Petroleum Science and Engineering*, 110, 268–293. https://doi.org/10.1016/j.petrol.2013.08.018
27. Nordbotten, J. M., Benali, B., Both, J. W., Brattekås, B., Storvik, E., & Fernø, M. A. (2024). Darsia: An open-source python toolbox for two-scale image processing of dynamics in porous media. *Transport in Porous Media*, 151(5), 939–973. https://doi.org/10.1007/s11242-023-02000-9
28. Nordbotten, J. M., Boon, W. M., Fumagalli, A., & Keilegavlen, E. (2019). Unified approach to discretization of flow in fractured porous media. *Computational Geosciences*, 23(2), 225–237. https://doi.org/10.1007/s10596-018-9778-9
29. Nordbotten, J. M., & Keilegavlen, E. (2021). An introduction to multi-point flux (Mpfa) and stress (Mpsa) finite volume methods for thermo-poroelasticity. In D. A. Di Pietro, L. Formaggia, & R. Masson (Eds.), *Polyhedral Methods in Geosciences* (pp. 119–158). Springer International Publishing. https://doi.org/10.1007/978-3-030-69363-3_4
30. Olasolo, P., Juárez, M. C., Morales, M. P., D´Amico, S., & Liarte, I. A. (2016). Enhanced geothermal systems (Egs): *A Review. Renewable and Sustainable Energy Reviews*, 56, 133–144. https://doi.org/10.1016/j.rser.2015.11.031
31. Rangel-German, E. R., & Kovscek, A. R. (2002). Experimental and analytical study of multidimensional imbibition in fractured porous media. *Journal of Petroleum Science and Engineering*, 36(1), 45–60. https://doi.org/10.1016/S0920-4105(02)00250-4
32. Rubner, Y., Tomasi, C., & Guibas, L. J. (1998). A metric for distributions with applications to image databases. *Sixth International Conference on Computer Vision* (IEEE Cat. No.98CH36271), 59–66. https://doi.org/10.1109/ICCV.1998.710701
33. Schädle, P., Zulian, P., Vogler, D., Bhopalam, S. R., Nestola, M. G. C., et al. (2019). 3D non-conforming mesh model for flow in fractured porous media using Lagrange multipliers. *Computers & Geosciences*, 132, 42–55. https://doi.org/10.1016/j.cageo.2019.06.014
34. Schwenck, N. (2015). An XFEM-Based Model for Fluid Flow in Fractured Porous Media. PhD thesis, University of Stuttgart.
35. Schwenck, N., Flemisch, B., Helmig, R., & Wohlmuth, B. I. (2015). Dimensionally reduced flow models in fractured porous media: Crossings and boundaries. *Computational Geosciences*, 19(6), 1219–1230. https://doi.org/10.1007/s10596-015-9536-1
36. Ţene, M., Bosma, S. B. M., Al Kobaisi, M. S., & Hajibeygi, H. (2017). Projection-based embedded discrete fracture model(Pedfm). *Advances in Water Resources*, 105, 205–216. https://doi.org/10.1016/j.advwatres.2017.05.009
37. Varela, J., Ahmed, E., Keilegavlen, E., Nordbotten, J. M., & Radu, F. A. (2023). A posteriori error estimates for hierarchical mixed-dimensional elliptic equations. *Journal of Numerical Mathematics*, 31(4), 247–280. https://doi.org/10.1515/jnma-2022-0038